Highlights

Direct measurements of Rayleigh wave acoustoelastic constants for shot-peened superalloys

Sergey Gartsev,Bernd Köhler

- Acoustoelastic constants (AEC), demanded for surface-treated alloy characterization using Rayleigh waves, may be obtained through direct measurements and indirect mapping using bulk wave AEC.

- Mapping between bulk and surface wave acoustoelastic constants (AEC) does not match up; therefore, the direct AEC measurements should be used for evaluation of the stress–strain state in the vicinity of the surface.

- Treatment may affect not only the RW AEC absolute value but also the sign.

- If ultrasonic testing NDE methods are used, the AEC must be determined for the given state of material (treatment and plastic deformation).

Direct measurements of Rayleigh wave acoustoelastic constants for shot-peened superalloys

Sergey Gartsev[a,*,1], Bernd Köhler[a]

[a]*Fraunhofer IKTS (Institut für Keramische Technologien und Systeme), Maria Reiche Straße 2, 01109 Dresden, Germany*

ARTICLE INFO

ABSTRACT

In this article, the experimental investigation of the dependency of surface wave (Rayleigh wave) acoustoelastic constants (AEC) on surface treatment parameters and plastic deformation is discussed. These constants are necessary for the monitoring of surface treatment intensity by means of ultrasonic testing. The indirect (mapping of bulk wave AEC to the surface wave AEC through the Grüneisen constants) method and the direct method are compared. Also the Rayleigh wave AEC have been directly measured for the different states of material (annealed, plastically deformed, or surface treated) for In718 and Ti6246 alloys. We show that surface AEC are very sensitive to any changes in material structure, up to changes in the sign of the effect, and for practical applications, the direct in-situ Rayleigh wave AEC measurement should be performed.

1. Introduction

Surface treatment, that is, a treatment of the surface and near-surface regions of a material to allow the surface to perform functions that are distinct from those functions demanded from the bulk of the material (ASM Handbook), is one of the essential aspects in the design of high-performance components in the aerospace industry [1]. Among the variety of different methods, the shot peening (SP), laser shock peening (LSP), and low plasticity burnishing (LPB) treatments allow for a significant increase in the high-cycle fatigue properties [2] and to improve foreign object damage resistance [3] for the gas turbine components.

The core of the aforementioned methods is the introduction of a compressive residual stress layer in the surface of a structural element (i.e., leading edge of fan blades or turbine disc), which retards the crack growth. SP, as the most convenient technique, is widely used during both the manufacturing and MRO (maintenance, repair, and operations) procedures, in order to improve the fatigue performance of elements and increase the life expectancy of an aircraft part.

Currently, industrial and in-field applications are used to validate the intensity of SP with a series of Almen stripes measurements—treated coupons with known properties. Semidestructive (borehole drilling) and destructive (slicing) methods are also used as reference. Only the laboratory NDE methods (electron, X-ray, or neutron diffraction) have proven its versatility for stress–strain state evaluation for a wide range of metals [4]. The motivation for the current research is to make developments regarding in-field nondestructive residual stress measurement tools.

The application of ultrasonic testing (UT) for evaluation of the material properties is one of the standard approaches [5]. In particular, the stress–strain state can be determined

with use of acoustoelastic effect—the dependency of the phase velocity of an elastic wave on the actual stress–strain state [6]. The change in the velocity is linked to stress through the material's nonlinear elastic properties, expressed as the acoustoelastic constants (AEC), or the third-order elastic constants (TOEC) [7, 8, 9, 10]. These constants have to be known either from the literature or by calibration with a known (e.g., applied) stress level. Defined first for the bulk wave in an isotropic solid, the theoretical description of the acoustoelastic effect has been extended for Rayleigh waves (RW) [11, 12], and also proved experimentally [13, 14].

As the residual stress level varies with depth [2], the use of Rayleigh waves appears beneficial due to the ability to control the penetration depth with the frequency. Published works indicate that estimation of the surface layer stress with the acoustoelastic effect is possible in principle; however, they also highlight the fundamental challenges [15, 16, 17, 18, 19, 20]. The main difficulty, in this case, is that the surface wave velocity is not only influenced directly by stress via the acoustoelastic effect but also by the microstructural changes due to plastic deformation (cold work). Therefore, at least two contributions affecting the Rayleigh wave velocity variation must be separated.

Moreover, the AEC, which express the material nonlinearity, are known to vary with the plastic deformation [15], which is also introduced by the surface treatment. Finally, only a few results for the relevant superalloys are available [16, 18, 19, 20, 21, 22].

As a combination of aforementioned factors, direct measurements of RW AEC are needed to gain more insight into the actual state of the material under test (i.e., residual stress–cold work contribution separation) before the residual stress profile may be reconstructed.

In this paper, we determine the Rayleigh wave AEC for the given samples, machined out of In718 and Ti6246, in two different ways. The first method is the direct measurement of the surface acoustic wave velocity under the different sample load states. The second, indirect way, is measuring the

material bulk wave AEC (BW AEC) and mapping these constants through known formulas for the isotropic materials to calculate the sequence BW AEC → TOEC → RW AEC.

The results obtained are compared with each other and with the few available literature values for the given materials. Even for annealed samples, the direct and mapped RW AEC values have shown a significant difference. Thus, there are direct AEC measurements for the samples with different treatment intensities: no treatment, 5 Almen, and 8 Almen (A). Direct measurements of RW AEC for the shot peened material were performed for the first time, to the best of the author's knowledge.

2. Theoretical background

In the general case of elastic wave propagation in an isotropic body, strained with uniaxial load in the direction '1', acoustoelastic constants can be defined as follows:

$$L_{ij} = \frac{\delta V_{ij}/V_{ij}^0}{\delta \epsilon} \tag{1}$$

where the first subindex shows the wave propagation direction in a Cartesian coordinate system, and the second subindex shows the particle dispacement direction for a given wave. ϵ is a strain level in direction '1', and V^0 stands for the velocity at zero axial strain.

The analytical expressions for the variation of velocity of the bulk wave in a pre-stressed isotropic solid were published first by Hughes and Kelly [6], based on Murnaghan's theory of finite deformations of solids [7]. According to that, dimensionless BW AEC for the case of uniaxial load, acting in a direction '1', may be written as [5]:

$$L_{21} = \frac{\lambda + 2\mu + m}{2(\lambda + \mu)} + \frac{\nu n}{4\mu} \tag{2}$$

$$L_{22} = -2\nu(1 + \frac{m - \mu l/\lambda}{\lambda + 2\mu}) \tag{3}$$

$$L_{23} = \frac{m - 2\lambda}{2(\lambda + \mu)} - \frac{n}{4\mu} \tag{4}$$

where λ and μ are the second-order elastic constants in Lame notation, ν is the Poisson ratio, and l, m, n are the third-order elastic constants (TOEC) in Murnaghan notation.

Therefore, AEC (or TOEC) may be determined for the given λ and μ with three independent measurements. In our case, the L_{22} has been measured with a pressure wave transducer, L_{21}, with a shear wave with particle displacement parallel to the load direction, and L_{23}, with a shear wave with particle displacement normal to the load direction (Figure 1). The values of the Lame constants have been obtained with velocity measurements with no load and a known density.

For the surface acoustic wave case, RW AEC can be defined, as in Equation 1 [12, 23]. An alternative definition is [14, 24]:

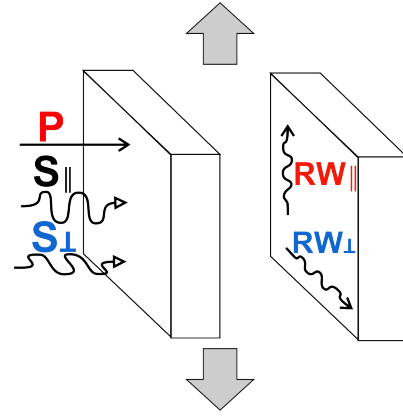$$\frac{\Delta V}{V} = \beta_{11}\sigma_{11} + \beta_{33}\sigma_{33} \tag{5}$$

Figure 1: Polarisation convention. Load direction 1 is shown with the grey arrows. Equations 2-4: $L_{21} \leftrightarrow S_\parallel$, $L_{22} \leftrightarrow P$, $L_{23} \leftrightarrow S_\perp$. Equation 5: $\beta_1 \leftrightarrow RW_\parallel$, $\beta_2 \leftrightarrow RW_\perp$
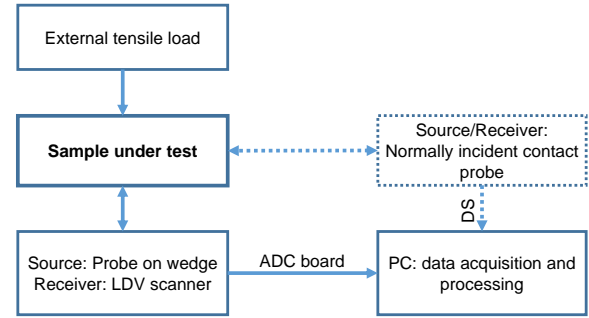

Figure 2: Principal measurement scheme (DS—Digital scope; LDV—laser Doppler vibrometer; ADC—analog-to-digital conversion). Bulk wave acoustoelastic constant (BW AEC) measurements are shown with a dashed line.

where the normal to surface is to be oriented in the '2' direction, with the dimension of β_{ii} of $[1/Pa]$.

A BW AEC can be linked with the RW AEC, through TOEC values via Grüneisen constants, which describe the strain dependence of the lattice vibrational frequencies ([25], Equation 4.22).

3. Samples and the experimental setup

The principal design of the experiment is shown in Figure 2. Four metal samples with two different shapes, machined from Inconel 718 and Titanium 6246 alloys, have been used for the measurements. At the first stage of the experiment, both samples have been plastically deformed (with $\sim 1\%$ maximum strain). Then, all of the samples were annealed and measured again. Finally, each sample was partially shot-peened with 5 Almen and 8 Almen intensity and the direct RW AEC measurements were performed again. The sample geometry and the surface-treated-area layout are shown in Figure 3.

In all measurements a ZwickRoell tensile machine has been used for the initiation of external uniform tensile strains on specimens at eight different levels at the ambient con-
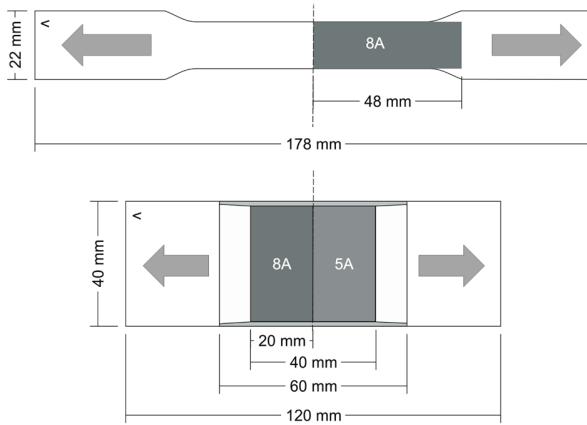
Figure 3: Samples geometry and shot peening (SP) scheme. Sample 1 (upper) is treated from both sides with intensity 5 Almen (A) and 8 A. Sample 2 (bottom) is peened from a single side. The sample 1 thickness is 4.8 mm, the sample 2 thickness is 3.8 mm. Load direction 1 is shown with gray arrows.

Figure 4: Rayleigh wave pulse shape and spectra for three commercial transducers with different f_c.

ditions. The actual strain of the sample was measured by means of a tensile machine extensometer. The effects related to sample heating, have been neglected.

For the measurement of BW AEC, the pressure and shear wave ultrasonic transducers, clamped normally to the sample surface, have been used both for the elastic wave generation and for the multiple echo signal recording. An excitation pulse was generated with a pulser-receiver (Olympus 5900PR). The received signal was conditioned with the same pulser-receiver and recorded with a high-end digital scope (LeCroy 62 Xi-A, 10 GS/s, 8 bit). For the evaluation of three AEC values for the isotropic material, BW measurements with the three possible polarisations have been performed (see the Figure 1 and the Equations 2–4). Each sample was measured at five different points.

For the direct RW AEC measurements, the ultrasonic transducer on a wedge was attached to the sample. The wedge angle was selected for the generation of the Rayleigh wave. Three commercial transducers with different nominal central frequencies f_c (1.5 MHz, 5 MHz, and 10 MHz) were used for the excitation. The waveform and the frequency spectra of the excited Rayleigh wave are presented for each transducer in Figure 4. For the recording of velocity variation, contactless laser Doppler vibrometer (LDV) scans were performed at several lines, parallel to the wave propagation direction. For the $RW_{\parallel}$ propagation direction, Sample 1 was used and both the excitation and recording were done at the same face. For the $RW_{\perp}$ case, Sample 2 was used, where the Rayleigh wave was generated at the backside and traveled around the half-round edge into the scan area (see also the [21] and Figure 3). The acquired signal was recorded with the analog-to-digital conversion (ADC) board (GaGe 14200, 200 MS/s, 8 bit).
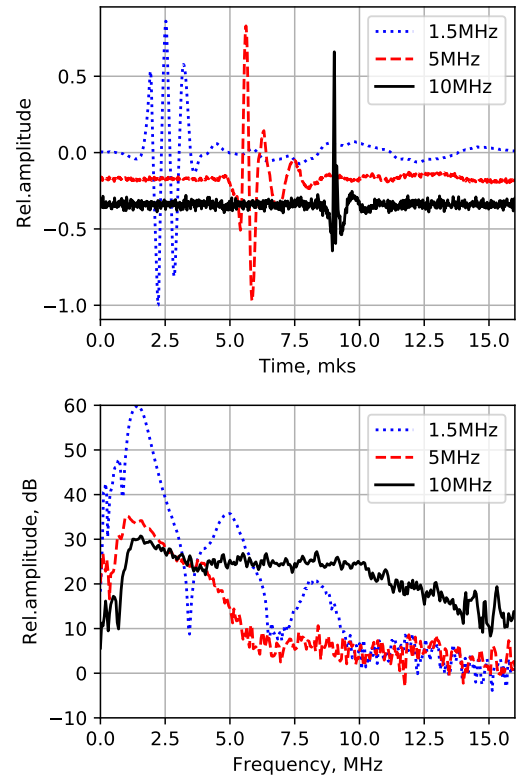
4. Data acquisition and processing

For both types of experiment, the broadband pulse signal was sent to the transducer with a given central frequency and bandwidth, and then, the delayed signal was recorded with several hundreds of averagings. The collected data were processed in the MATLAB and Python 3.7 environments. With several variations, dependent on data acquisition systems, the general processing strategy looked as follows:

1. Raw data filtering in the bandwidth of interest with FIR (finite impulse response) or DWT (discrete wavelet transform) filter.
2. Extracting the cross-correlation function peaks time delay.
3. Propagation velocity estimation based on the line fit in the (real travel path, cross-correlation peak delay) space.

The influence of probe/wedge geometry was neglected for both cases.

4.1. Bulk waves

The multiple echo signal was recorded with a high-resolution digital scope, allowing us to accurately extract the elastic wave velocity for the relatively short traveling distance. An example of the recorded multiple-echo signal and extracted cross-correlation peaks is shown in Figure 5. For each of the three possible polarizations, the dependency of the velocity variation on applied loads was measured at five
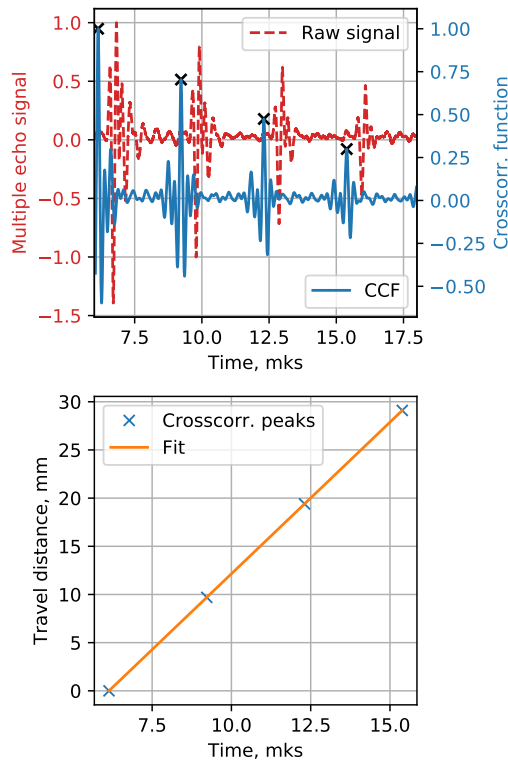
Figure 5: Multiple echo signal processing example.

Table 1
Third-order elastic constants (TOEC) values, calculated from measured BW AEC, and a comparison with the literature values.

Material	l, GPa	m, GPa	n, GPa
In718 (5 points)	-556±5	-624±5	-484±5
In718 (3 points) [19]	-524±4	-603±4	-478±2.3
In718 (3 points) [22]	-472±19	-564±15	-489±7
Ti6246 (5 points)	-312±125	-309±71	-442±51
Ti6246 (3 points) [19]	-356±35	-390±21	-475±15

different points. The results of the measurements are shown in Table 1 and Figure 6.

4.2. Rayleigh waves

For the extraction of the surface acoustic wave velocity dependence on the applied load, a series of contactless scans were performed with a LDV (laser Doppler vibrometer), mounted on the 3-axis scanner. The acoustoelastic constants have been measured for the Rayleigh wave, traveling parallel and normal to the load direction. The recorded propagation distance for the treated and non-treated cases was in the range of 30–45 mm for the different sample types. The out-of-plane component of displacement was scanned along five to eight parallel lines with a 1 mm step and 1 mm line offset. The additional procedure for the velocity extraction was needed, due to the rather low SNR (signal-to-noise ratio) level of the LDV measurements, especially for the treated
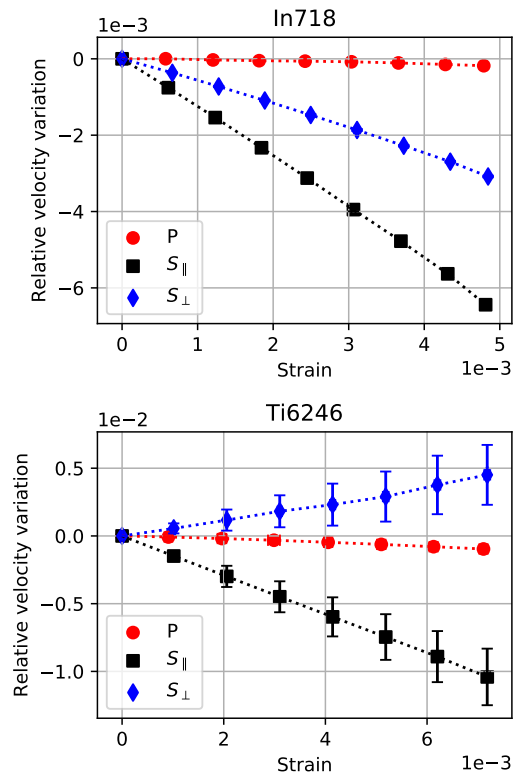

Figure 6: Bulk wave AEC measurement results for 5 different points for the In718 and Ti6246 alloys

samples at higher frequencies. Each scan line was treated independently as a B-scan, and processed as follows:

1. Selection of the point with the highest SNR (reference point).
2. Calculation of the cross-correlation function between the reference point and given point at the scan line.
3. Extraction of the cross-correlation function maximum time delay (between the reference point and given point).
4. Estimation of the RW velocity by the linear approximation in the (scanner coordinate–cross-correlation peak delay) space with an iterative algorithm, the random sample and consensus (RANSAC) [26].

RANSAC, or random sample and consensus algorithm, is an iterative algorithm to estimate the model parameters in the presence of *outliers*. In the present case, outliers were defined as points with an SNR lower than the threshold level, or the secondary peaks, extracted from the cross-correlation function. In general, RANSAC consists of two iterative stages:

1. Select the random minimal sample set (*2 points for the line scan*) from the input dataset (*B-scan*) to fit the model.
2. Add the points to the sample set, which are consistent with the model with a predefined error.

The procedure is stopped if the fit quality target value or the maximum number of iterations is reached. The threshold and fit quality parameters have been selected manually. An
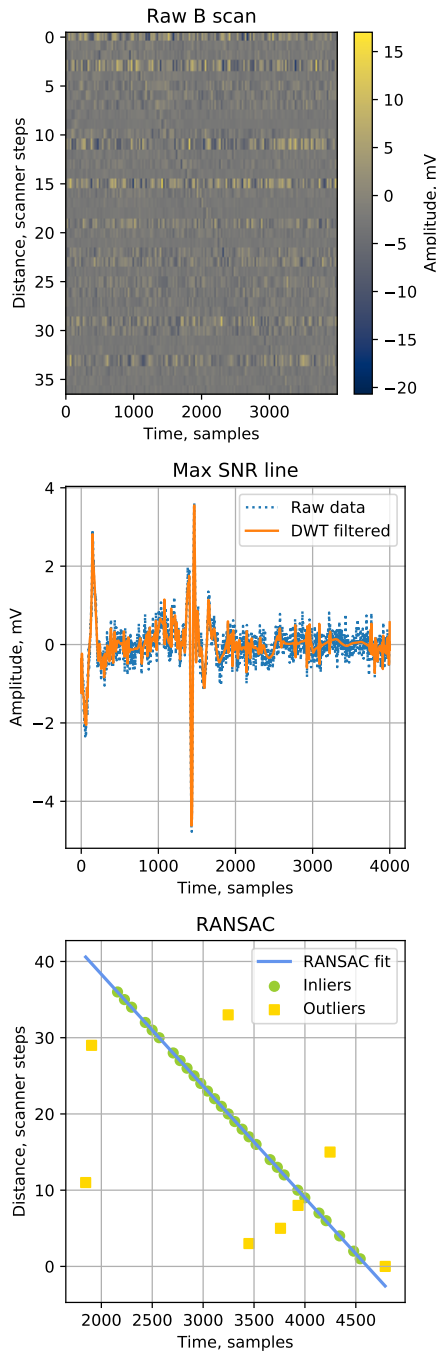
Figure 7: B scan processing example. Upper figure—raw B-scan; middle figure—raw record at the given point and result of filtering; bottom figure—result of iterative fitting.

Figure 8: Results of the measurements of β_{33} for In718 at f_c=5MHz).

Table 2
Direct-measured RW AEC for the different states of material and comparison with the literature and mapped values (here, PD—plastically deformed; AA—after annealing; BW: mapped from the TOEC values, available literature values are shown with the reference number).

Material	f_c(MHz)	$\beta_{11}(1/TPa)$	$\beta_{33}(1/TPa)$
In718 (PD)	1.5	-4.11 ± 3.89	-1.73 ± 3.03
In718 (AA)	1.5	3.39 ± 0.66	-0.92 ± 0.77
In718 ([21])		2.36	-1.20
In718 (BW)		2.18 ± 0.07	-1.31 ± 0.03
In718 (0A)	1.5	-0.49± 0.78	
In718 (0A)	5	0.38 ± 2.90	-7.98 ± 1.47
In718 (0A)	10	0.23 ± 2.81	
In718 (5A)	5	-1.27 ± 2.80	-6.88 ± 2.48
In718 (5A)	10	-0.95 ± 1.84	
In718 (8A)	5	-2.40 ± 4.33	-2.51 ± 1.80
In718 (8A)	10	6.06 ± 1.25	
Ti6246 (PD)	1.5	0.32 ± 2.60	-2.36 ± 3.20
Ti6246 (AA)	1.5	3.36 ± 0.25	1.46 ± 2.10
Ti6246([21])		2.79	1.62
Ti6246 (BW)		3.3 ± 2	5.81 ± 1.97
Ti6246 (0A)	5	7.83 ± 4.19	1.61 ± 1.22
Ti6246 (5A)	5	6.25 ± 4.42	3.65 ± 1.72
Ti6246 (8A)	5	3.42 ± 3.59	7.66 ± 2.99

example of the B-scan processing with the RANSAC algorithm is shown in Figure 7.

An example of velocity variation extraction for the β evaluation for the In718 is shown in Figure 8.

5. Results

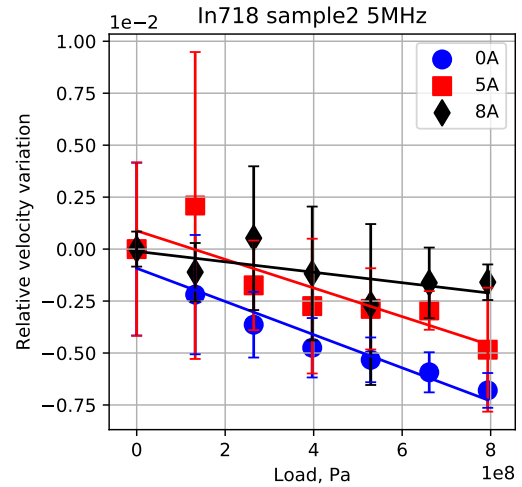TOEC vaues, mapped from the direct BW AEC measurements, and the comparison with the published results are given in Table 1. The available results for the In718 sample are in good correlation with the measured values. The high scattering of Ti6246 nonlinear elastic constant values was expected from previous works [19], and can be explained by the variation in the microstructural properties, which is beyond the scope of the current work.

The results of RW AEC extraction for the samples with different treatment histories are shown in Table 2. A different history means the same samples have been measured after plastic deformation, annealing, and shot-peening. This
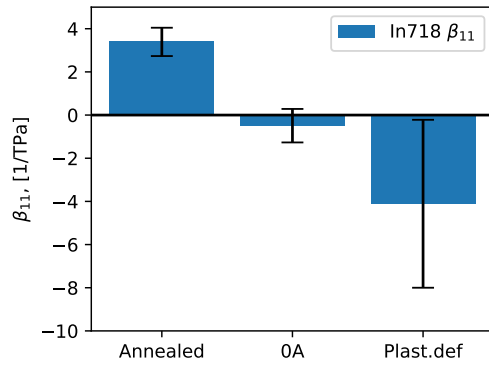
Figure 9: In718 β_{11} evolution for three different sample states, f_c=1.5 MHz. (0 A—nontreated part of the treated sample).
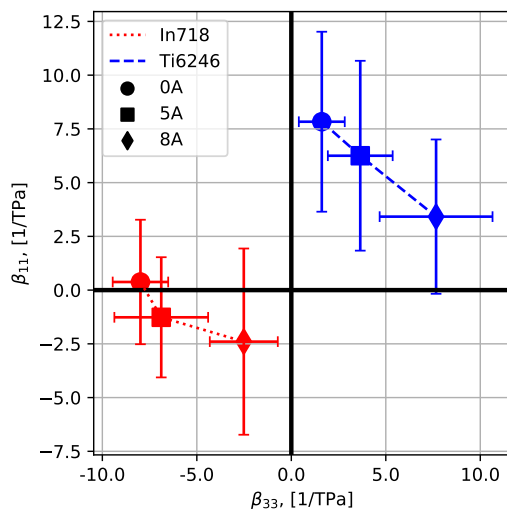

Figure 10: RW AEC variation for 0 Almen (nontreated), 5 Almen, and 8 Almen shot-peening intensity for In718 and Ti6246 alloys, $f_c = 5$ MHz. Vertical axis—β_{11}; horizontal axis—β_{33}

table includes the values, mapped from the annealed sample BW AEC measurements (according to [25]), and the few published results. Mapping was done with the Lame constants, obtained with the literature values for density and the BW velocity measurements at the zero load (ρ_{In} = 8220 kg/m^3, V_{In}^P = 5814 m/s, V_{In}^S = 3096 m/s, ρ_{Ti} = 4650 kg/m^3, V_{Ti}^P = 6126 m/s, V_{Ti}^S = 3150 m/s). As can be seen, the measured values of the β constants are dependent on the material state. Mapping of BW AEC (indirect measurement method) yields the close results only for the β_{11}^{Ti}. The reasons of deviation of the rest mapped RW AEC from the directly measured values needs further investigation.

In Figure 9, the parameter β_{11}, measured for the three different states of the single In718 sample, is depicted with a vertical bar chart. These states are shown on the horizontal axis: the sample after annealing, after the partial surface treatment (measurements done at nontreated area), and after the plastic deformation. Due to the apparent anomaly behavior, measurements for the 0A state have been repeated

for several times, but always have shown the similar result. Both the magnitude and the sign of RW AEC are dependent on the In718 alloy treatment history.

The effect of the shot-peening intensity on the sign and value of RW AEC for In718 and Ti6246 is depicted in Figure 10. In contrast with the titanium alloy, for which the 'cumulative' nonlinearity $\beta_{11}+\beta_{33}$ maintains the sign and magnitude, for the Inconel, both β constants undergo severe variations in magnitude and/or sign, therefore jeopardizing its following application for the surface-treated structure residual stress evaluation.

6. Discussion

In this paper, the problem of estimating the acoustoelastic constant of surface acoustic waves for mechanically processed superalloys has been considered. For the characterization of the surface treatment intensity with the use of ultrasonic waves, one should always account for the state of the material, penetration depth or bandwidth of interest, and wave propagation orientation.

The necessity of use of direct measurements has been shown through comparison with the BW AEC values, measured for the same samples and mapped to the RW AEC. In the given case, the existing theoretical model failed to predict the values obtained through direct measurement, except for the β_{11}^{Ti} case.

As shot-peened superalloys, RW AEC are highly sensitive to the treatment intensity and RW penetration depth. Thus, the aforementioned parameters should be determined in the actual region of interest, taking into account both the macro- and micro-structure of the material under test. The influence of the surface treatment on nonlinear elastic properties varies with the alloy type as well. Inconel alloy RW AEC tend to have stronger variations with the shot peening intensity, than the titanium alloy does.

Therefore, for practical applications—for example, for the retrieval of information regarding the treatment condition and the stress–strain state—the development of an infield RW AEC measurement method is essential.

References

[1] W. Zhuang, B. Wicks, Mechanical surface treatment technologies for gas turbine engine components, Journal of Engineering for Gas Turbines and Power 125 (2003) 1021–1025.

[2] L. Wagner, Mechanical surface treatments on titanium, aluminum and magnesium alloys, Materials Science and Engineering: A 263 (1999) 210–216.

[3] T. E. Pistochini, M. R. Hill, Effect of laser peening on fatigue performance in 300m steel, Fatigue & Fracture of Engineering Materials & Structures 34 (2011) 521–533.

[4] P. Withers, H. Bhadeshia, Residual stress. part 1 – measurement techniques, Materials Science and Technology 17 (2001) 355–365.

[5] D. E. Bray, R. K. Stanley, Nondestructive evaluation: a tool in design, manufacturing and service, CRC press, 1996.

[6] D. S. Hughes, J. L. Kelly, Second-order elastic deformation of solids, Physical Review 92 (1953) 1145–1149.

[7] F. Murnaghan, Finite Deformation of an Elastic Solid, New York (1951), John Wiley and Sons, 1951.

[8] L. Landau, E. Lifshitz, Theory of elasticity, 3rd, Pergamon Press 3 (1986).

[9] D. Husson, G. S. Kino, A perturbation theory for acoustoelastic effects, Journal of Applied Physics 53 (1982) 7250–7258.

[10] S. Takahashi, R. Motegi, Stress dependency on ultrasonic wave propagation velocity, Journal of Materials Science 22 (1987) 1857–1863.

[11] Y. Iwashimizu, The rayleigh wave in a finitely deformed isotropic elastic material, The Journal of the Acoustical Society of America 64 (1978) 910.

[12] M. Hirao, H. Fukuoka, K. Hori, Acoustoelastic effect of rayleigh surface wave in isotropic material, Journal of Applied Mechanics 48 (1981) 119–124.

[13] A. Zeiger, K. Jassby, Measurement of acoustoelastic coefficients of rayleigh waves in steel alloys, Journal of Nondestructive Evaluation 3 (1982) 115–124.

[14] D. Husson, A perturbation theory for the acoustoelastic effect of surface waves, Journal of Applied Physics 57 (1985) 1562–1568.

[15] P. B. Nagy, Opportunities and challenges for nondestructive residual stress assessment, in: AIP Conference Proceedings, AIP, 2006. doi:10.1063/1.2184508.

[16] B. Köhler, M. Barth, F. Schubert, J. Bamberg, H.-U. Baron, D. O. Thompson, D. E. Chimenti, Characterization of surface treated aero-engine alloys by rayleigh wave velocity dispersion, in: Conference, AIP, 2010. doi:10.1063/1.3362402.

[17] M. Liu, J.-Y. Kim, L. Jacobs, J. Qu, Experimental study of nonlinear rayleigh wave propagation in shot-peened aluminum plates—feasibility of measuring residual stress, NDT & E International 44 (2011) 67–74.

[18] M. Barth, M. Küttner, B. Köhler, J. Bamberg, H.-U. Baron, Universal ultrasonic goniometer for rayleigh and surface skimming longitudinal wave dispersion measurements, in: Conference, AIP, 2012. doi:10.1063/1.4716439.

[19] M. Rjelka, M. Barth, S. Reinert, B. Koehler, J. Bamberg, H. U. Baron, R. Hessert, Third order elastic constants and rayleigh wave dispersion of shot peened aero-engine materials, Materials Science Forum 768-769 (2013) 201–208.

[20] S. Hubel, A. Dillhöfer, H. Rieder, M. Spies, J. Bamberg, J. Götz, R. Hessert, C. Preikszas, Ultrasonic evaluation of residual stresses in aero engine materials using bulk and rayleigh surface waves, AIP Publishing LLC, 2014. doi:10.1063/1.4864876.

[21] B. Köhler, M. Barth, J. Bamberg, H.-U. Baron, Rayleigh wave velocity dispersion for characterization of surface treated aero engine alloys, in: Proceedings of the ECNDT, 2010.

[22] S. Hubel, M. Spies, H. Rieder, A. Dillhoefer, J. Bamberg, R. Hessert, C. Preikszas, Basic investigations to establish an ultrasonic stress evaluation technique for aero engine materials, NDT in Aerospace 2012 - Th.1.B.3 (2012).

[23] Y.-C. Lee, J. O. Kim, J. D. Achenbach, Measurement of stresses by line-focus acoustic microscopy, Ultrasonics 32 (1994) 359–365.

[24] M. Duquennoy, M. Ouaftouh, M. Ourak, F. Jenot, Theoretical determination of rayleigh wave acoustoelastic coefficients: comparison with experimental values, Ultrasonics 39 (2002) 575–583.

[25] A. P. Mayer, Surface acoustic waves in nonlinear elastic media, Physics Reports 256 (1995) 237–366.

[26] S. Choi, T. Kim, W. Yu, Performance evaluation of RANSAC family (2009).